Two-Way Photonic Interface for Linking the Sr^+ Transition at 422 nm to the Telecommunication *C* Band

Thomas A. Wright,[1,*] Robert J. A. Francis-Jones,[1,2] Corin B. E. Gawith,[3] Jonas N. Becker,[2] Patrick M. Ledingham,[2] Peter G. R. Smith,[3] Joshua Nunn,[1] Peter J. Mosley,[1] Benjamin Brecht,[2] and Ian A. Walmsley[2]

[1] *Centre for Photonics and Photonic Materials, Department of Physics, University of Bath, Bath BA2 7AY, United Kingdom*

[2] *Clarendon Laboratory, University of Oxford, Parks Road, Oxford OX1 3PU, United Kingdom*

[3] *Optoelectronics Research Centre, University of Southampton, Southampton SO17 1BJ, United Kingdom*

(Received 13 June 2018; revised manuscript received 16 August 2018; published 4 October 2018)

We report a single-stage bidirectional interface capable of linking Sr^+ trapped-ion qubits in a long-distance quantum network. Our interface converts photons between the Sr^+ emission wavelength at 422 nm and the telecom *C* band to enable low-loss transmission over optical fiber. We have achieved both up- and down-conversion at the single-photon level with efficiencies of 9.4% and 1.1%, respectively. Furthermore, we demonstrate noise levels that are low enough to allow for genuine quantum operation in the future.

DOI: 10.1103/PhysRevApplied.10.044012

I. INTRODUCTION

Large-scale quantum networks suitable for long-distance secure communication and distributed computation require not only that quantum information may be manipulated reliably, but also communicated successfully between remote nodes [1,2]. However, existing quantum-information-processing platforms are not individually able to fulfill both of these requirements. For example, photons can distribute quantum information through fiber networks [3] or via satellite [4] but multiphoton gates remain challenging, whereas trapped ions have achieved high-fidelity two-qubit operations [5] but are unsuitable for sharing entanglement beyond a single laboratory. However, integrating disparate technologies to form a hybrid light-matter quantum network promises the capability to carry out entanglement distribution and quantum communication over long distances [6,7].

The optical communication bus between nodes must overcome two technical challenges: compatibility between devices operating at different optical frequencies and low loss across large separations. Quantum frequency conversion (QFC), where a photon is coherently shifted to a different frequency band, addresses this difficulty by linking wavelengths as short as the ultraviolet (UV), where many convenient ion transitions are located, and the infrared (IR) telecommunications bands, enabling long-distance low-loss transmission in optical fiber [8].

A diverse range of platforms have been utilized to demonstrate frequency conversion via three- or four-wave mixing, including nonlinear crystals [9,10], planar waveguides [11,12], optical fibers [13,14], microresonators [15,16], and atomic systems [17,18]. QFC experiments initially focused on enhancing detection of IR photons by mapping them to the visible and near-infrared (NIR), where efficient silicon photon detectors existed [9,19]. QFC has since been shown to achieve the frequency remapping of both squeezed light [20,21] and entangled states [12,22]. The enhancement offered by QFC to optical interconnects within a quantum network has led to a demonstration of direct coupling between dissimilar quantum memories [23], as well as a multitude of experiments translating node-compatible photons both from [12,20,24–30] and to [22,31–40] different telecommunication bands.

Near-unit efficiency frequency conversion has been demonstrated [14], although, in practice, complexities arising from photon bandwidth, pump-induced noise, and the required frequency shift have limited the capability of many converters, proving arduous challenges to overcome. QFC via three-wave mixing, in particular, imposes

*t.wright@bath.ac.uk

the strict requirement that the high nonlinear coupling be provided by a singular strong pump, which, additionally, must account for the energy difference between the input and target wavelength. In large part, existing QFC experiments have exploited opportune laser wavelengths and transitions predominantly in the red and NIR. The large frequency separation between IR and the blue or UV makes connecting most ion traps to the telecom bands particularly challenging, leading to the proposition of a two-stage approach [41]. Classical generation of UV light by means of parametric three-wave mixing is in itself difficult and so far has been realized by second harmonic generation (SHG) [42] and sum frequency generation (SFG) [43]. Recently however, developments in the translation of quantum states between ultraviolet and the O band have been shown [44,45], albeit only in one direction. The majority of reported conversions thus far have been unidirectional with limited exceptions [46], whereas to create a functional quantum network in fiber, shifting to the telecoms is critical and two-way conversion is desirable.

We report the realization of single-stage bidirectional frequency conversion at the single photon level for interfacing the $S_{1/2} \rightarrow P_{1/2}$ transition in trapped Sr^+ ion qubits (422 nm) with the telecommunication C band (1550 nm). The conversion is achieved in a magnesium-doped periodically poled lithium niobate (MgO:PPLN) crystal, where $\chi^{(2)}$ sum or difference frequency generation (DFG) can be used to achieve up or down conversion of an input photon. By monitoring the conversion of weak coherent light with single-photon detectors, we demonstrate that the noise level, expressed as the actual noise photons normalized to the conversion efficiency, μ_1 [47], is as low as 0.0185—far below the level required for use as the interface in a hybrid quantum network. This is to our knowledge the only bidirectional link between blue ion transitions and the C band.

II. TECHNICAL DETAILS

In order to map the input to the target output wavelength, a strong pump field must be tuned to fulfill the energy conservation requirement $\hbar\omega_{\text{in}} + \hbar\omega_{\text{pump}} = \hbar\omega_{\text{out}}$ for SFG up-conversion and $\hbar\omega_{\text{in}} - \hbar\omega_{\text{pump}} = \hbar\omega_{\text{out}}$ for DFG down-conversion. In both SFG and DFG, the amplitude of the strong pump serves to drive the nonlinear optical response facilitating the conversion. The efficiency of the process is related to the strength of the coupling between the fields in the QFC Hamiltonian:

$$\hat{\mathcal{H}} = i\hbar\kappa A_{\text{pump}}(\hat{a}^{\dagger}_{\text{out}}\hat{a}_{\text{in}} - \text{H.c.}), \tag{1}$$

determined by the parameter κ, which itself is dependent on the magnitude of the fields but also on their relative phase, the spatial overlap in the crystal, and the intrinsic nonlinearity of the material [8].

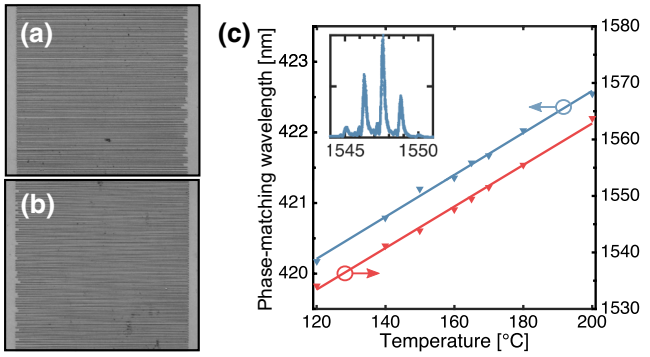

FIG. 1. Optical micrographs of the (a) $+z$ and (b) $-z$ surface of one of the 3.75-μm periodically poled MgO:$LiNbO_3$ crystals. (c) Phase-matching characteristics. The temperature response of the phase matching of the 3.75-μm poled crystal, i.e., the wavelength of perfect phase matching as a function of crystal temperature. Inset: SFG phase-matching curve, i.e., short-wavelength output power as a function of the input telecom wavelength at a constant crystal temperature and pump power.

For such widely separated wavelengths, the large wave-vector mismatch Δk between the propagation constants of the three fields means that phase matching is difficult to satisfy in commonly available materials. Even typical quasi-phase-matched (QPM) crystals that achieve efficient conversion when

$$\Delta k - \frac{2\pi}{\Lambda} = k_{\text{out}} - k_{\text{in}} - k_{\text{pump}} - \frac{2\pi}{\Lambda} = 0, \tag{2}$$

have a poling pitch Λ that is too long to compensate the large Δk in our interaction. Hence, we use a MgO:PPLN crystal fabricated in collaboration with Covesion Ltd. with ferroelectric domains created using a proprietary electric-field poling technique to produce a very short pitch, shown in Fig. 1. A photoresist pattern is created on the $-z$ (bottom) face of a 0.5-mm-thick, single-domain, z-cut, 3-inch-diameter MgO:$LiNbO_3$ crystal wafer. Liquid electrodes are applied to both the patterned $-z$ and unpatterned $+z$ surfaces of the crystal to enable electrical contact with the wafer surface. Domain inversion along the z axis is performed at room temperature by voltage-controlled application of an electric field based on a first stage of domain nucleation above the coercive field of the crystal, and a second stage of domain spreading near the coercive field (~ 4.5 kV mm^{-1}); this technique results in inverted domains that traverse the entire thickness of the crystal. The MgO:PPLN wafer is diced and polished into multiple chips, each containing five 300 μm-wide gratings with periods of 3.75, 3.85, 3.95, 4.05, and 4.15 μm, respectively. These periods are calculated to enable SFG and DFG processes between 422 nm and the telecom C band. The MgO:PPLN crystal used in this experiment is 19.97 mm long, with the 3.75-μm grating selected; it is not antireflection coated.

III. EXPERIMENTAL DEMONSTRATION

A. Phase-matching characterization

The experimental setup for characterizing the SFG up-conversion is shown in Fig. 2(a). An 80-MHz synchronously pumped tunable dye laser operating at 580-nm wavelength and 30-ps pulse duration (Sirah Gropius) is used to pump the conversion and a tunable continuous-wave (CW) laser with a 40-MHz linewidth (Santec TSL-510 C) provides a coherent IR input that is attenuated to low mean photon number. The pump and input beam size and polarization are set using telescopes, polarizing beam splitters (PBSs), and half-wave plates (HWPs) before the beams are combined at a dichroic mirror (DM) and directed toward the MgO:PPLN crystal. A pair of fused silica lenses is then used to focus the overlapped beams into the crystal. Care is taken to balance matching the Rayleigh length of each beam to half the crystal length while minimizing the difference between the cross sections of the beam waists. Following the crystal, a flipper mirror allows for the input and pump powers transmitted through the crystal to be measured. The pump, unconverted IR input light, and successfully converted violet output are then separated using a series of dichroic and short-pass filters (SPFs) before being directed to two single-photon avalanche diodes (SPADs). At the short wavelength, the pump light is removed using short-pass filters at 500 and 440 nm as well as a short-pass dichroic filter with an edge at 500 nm. The remaining signal is monitored by a blue-enhanced Si SPAD with a detection efficiency, dead time, and dark count rate of 86%, 43 ns, and 6 Hz, respectively. For the long wavelength we utilize a fiber-coupled InGaAs SPAD operating at 9.5% detection efficiency with a dead time of 10 μs. A time-tagging module (TTM) is used to record counts from the detectors. A spectrograph with electron-multiplying CCD camera is available to monitor the spectra of the violet light.

In order to maximize the coupling constant κ, the phase matching of the crystal is first characterized. With the temperature of the crystal stabilized at 160°C, the input IR beam is swept in wavelength while the intensity of the converted violet light is measured, mapping out the phase-matching curve, for a pump wavelength of 579.6 nm. We observe several distinct peaks in the phase matching (see Fig. 1), indicative of either multiple frequency modes within the pump beam or inhomogeneous poling across the length of the crystal.

We measure the change in position of the central phase-matching peak as a function of temperature, for a range of crystal temperatures, by sweeping the input wavelength while measuring the output violet power using an amplified photodiode. For the input IR light, we measure a temperature response of $\Delta\lambda_{\text{in}}/\Delta T = 0.4$ nm/K, corresponding to a change in the output wavelength of $\Delta\lambda_{\text{out}}/\Delta T = 0.0297$ nm/K.

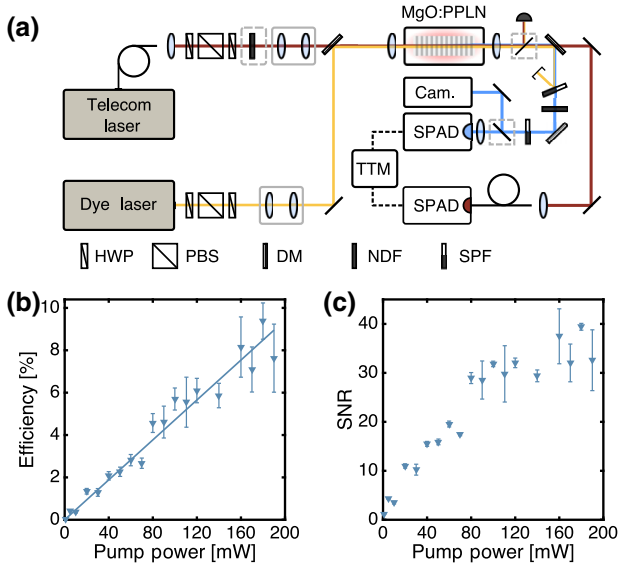

FIG. 2. (a) Experimental setup of the SFG up-conversion. (b) Up-conversion efficiency of the interface. (c) Signal-to-noise ratio of the up-conversion.

B. Frequency up-conversion

Having established the phase-matching response of the crystal, we investigate the achievable up-conversion efficiency. IR light at 1547.6 nm is converted to 421.7 nm by pumping the process at 579.6 nm with a fixed crystal oven temperature of 160°C.

We present the external efficiency η_{ext} of the SFG conversion in Fig. 2(b), which we define as the mean number of converted photons per second leaving the crystal divided by the number of input photons per second incident and temporally overlapped with the pump. The number of input photons per second, $\langle n\rangle_{\text{in}}$, is therefore given by

$$\langle n\rangle_{\text{in}} = (P_{\text{in}}D)/(\hbar\omega_{\text{in}}), \tag{3}$$

where P_{in} is the IR power transmitted through the crystal measured with the pump beam blocked. Because of observations of drift in the IR input power, P_{in} is measured both before and after each integration over which we record detector counts and is subsequently used to calibrate changes in the IR light level at the InGaAs SPAD. Because of the CW nature of the input light, the duty cycle D is defined as the pump pulse width multiplied by the repetition rate: $D = \tau_{\text{pump}}R_p$.

The conversion efficiency is then calculated as

$$\eta_{\text{ext}} = (S - N)/(\langle n\rangle_{\text{in}}\eta_{\text{loss}}), \tag{4}$$

where η_{loss} incorporates the detector efficiency (86%); transmission through optical components (96%); and, at higher powers, a neutral density filter (NDF) with approximately 20% transmission used to prevent detector saturation. S and N are the signal and noise counts per second,

respectively. As the SPAD detectors output only a single click when one or more photons arrive within their dead time, S and N are corrected relative to the measured rates S_{raw} and N_{raw} as follows:

$$S = \frac{S_{\text{raw}}}{1 - S_{\text{raw}} T_D}; \quad N = \frac{N_{\text{raw}}}{1 - N_{\text{raw}} T_D}, \tag{5}$$

where $T_D \gg 1/R_p$ is the dead time of the detector. The background noise is measured by blocking the IR input and recording counts at the visible detector with the pump unblocked.

In order to demonstrate the capability of the interface to operate at low photon numbers, we set a target input of overlapping an average of two IR photons from the IR-attenuated coherent source with every pump pulse. The resulting conversion efficiency is shown in Fig. 2(b). The highest measured external efficiency of $\eta_{\text{ext}} = 9.4 \pm 0.86\%$ is observed for an average pump power of 180 mW. Each point in Fig. 2(b) corresponds to a measurement consisting of between 5 and 10 s of integration, beyond which we observe a drop in efficiency. This is later realized to be due to the absorption of the pump light causing localized heating of the crystal, resulting in a change in the phase matching. The phenomenon of pump-power-induced change in Δk for $\chi^{(2)}$ QFC processes has been discussed previously [45,48]. Additional change in the phase mismatch is also introduced due to the photorefractive effect and, as such, when operating over extended periods of time as would be required in a network, the process would be pumped at a constant power, with the phase-matching-temperature tuning being optimized at the selected pump power. Figure 2(c) shows the signal-to-noise ratio (SNR) achieved across a range of pump powers, where we define $\text{SNR} = S/N$. The SNR achieved for the point at which we achieve highest conversion is 39.4 ± 0.69.

C. Frequency down-conversion

In order to demonstrate a two-way interface, we similarly characterize the reverse process, converting single-photon-level violet light to IR via DFG. Figure 3(a) shows the modified experimental setup. The input light at 425.5 nm is obtained by second harmonic generation of an 80-MHz repetition rate Ti:sapphire laser operating at 851-nm wavelength and 300-ps pulse duration (Spectra Physics Tsunami), which is synchronized to the clock signal of the dye laser system via an active cavity-length control. Replicating the interface between 421.7 nm and the C band is not possible due to the phase-matching restriction of the SHG crystal. In order to successfully translate the violet light to the telecom C band, we tune the wavelength of the dye laser to 585 nm and adjust the crystal oven temperature to 226.4°C. This enables us to optimize conversion to 1560.6 nm. Mitigation of the pump-induced change

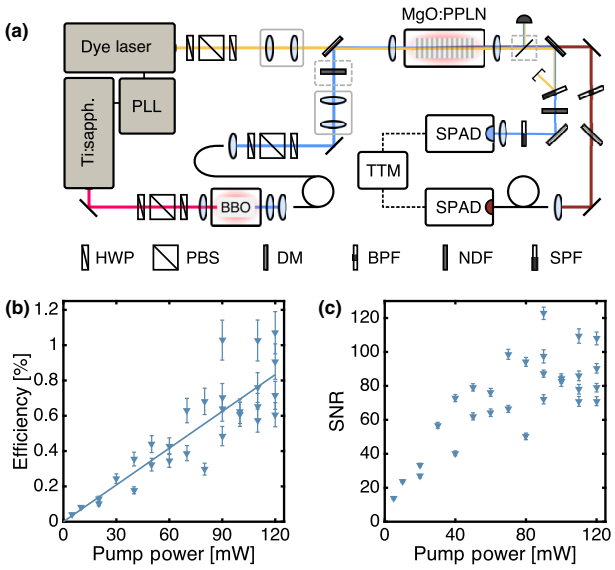

FIG. 3. (a) Experimental setup of the DFG down-conversion. PLL denotes phase-locked loop. (b) Down-conversion efficiency of the interface. (c) Signal-to-noise ratio of the down-conversion.

in Δk is achieved by optimizing the oven temperature while pumping the nonlinear conversion with an average power of 60 mW, half of the available range. In the long-wavelength detection arm, the filtering consists of two long-pass filters with edges at 950 and 650 nm. An 8.9-nm-wide band-pass filter (BPF) is used, centered at 1570 nm and rotated in order to shift the transmission to accommodate the converted light at 1560 nm.

In Fig. 3(b), we present the external efficiency of the conversion, where we have accounted for sources of loss outside the crystal, as described by Eq. (1). We evaluate η_{loss}, incorporating the detector efficiency (approximately 9.5%), transmission through optical components (approximately 73%), and fiber coupling efficiency (approximately 65%). The duty cycle D is defined as the ratio of the pump and input pulse durations: $D = \tau_{\text{pump}}/\tau_{\text{input}}$. The same target input photon number as the SFG conversion, of $\langle n \rangle_{\text{in}} = 2$ per pulse, is used in the DFG experiment. Across the data collected, counts are measured for integration times longer than 15 s.

The pump and input beam are steered using mirrors ahead of the crystal to optimize the beam overlap, leading to a wide distribution of observed conversion at comparable pump powers. A maximum external conversion efficiency of $(1.1 \pm 0.12)\%$ is achieved for a pump power of 120 mW. While significantly lower than the approximately 6% external efficiency observed for the SFG at equal pump power, the observed value may be partly explained by a change in beam waist between the two experiments. The beam waist of the pump in both experiments is approximately 43.2 μm, while the input light beam waist is increased from approximately 63.3 μm in

the SFG up-conversion to approximately 112 μm in the DFG down-conversion. This indicates that the maximum proportion of the input overlapped by the pump changes from approximately 46.6% to 14.9%. It could be expected that further optimization of the optics selection may yield improved conversion efficiencies, in particular when considered for the DFG down-conversion. Again, we draw attention to the conversion efficiency being limited by the available pump power in the experiment, as can be seen from the linear slope of the efficiency vs pump power curve in Fig. 3(b). The down-conversion is shown to have low noise in operation, with a SNR of 108 ± 3.8 measured at the point of highest conversion.

IV. DISCUSSION

A. Noise analysis

In order to demonstrate that our device is capable of operating as a QFC interface in a quantum network, for both up- and down-conversion, we calculate the mean input photon number per pulse that would yield a SNR $= 1$, commonly referred to as μ_1 [47]. Originally defined for quantum memories, the parameter μ_1 provides a useful performance benchmark for frequency conversion as it normalizes the noise by the conversion efficiency, thus precluding noise reduction by pumping with unrealistically low power. The calculated values are shown in Fig. 4(a). For the up-conversion, we find the minimum $\mu_1 = 0.05074$ when operating at a pump power of 180 mW. We note that this value is limited by the pump power in the experiment, as can be seen from the linear slope of the efficiency vs pump power curve, and that these values are obtained without narrow-band spectral filtering. For the down-conversion, we find $\mu_1 = 0.0185$ at a pump power of 120 mW.

The very low value of μ_1 for down-conversion shows that noise originating from broadband, un-phase-matched spontaneous parametric down-conversion (SPDC) of the pump field—typically a limiting factor in $\chi^{(2)}$ QFC schemes linking short to long wavelengths [49]—does not inhibit the capability of our system to operate at the single-photon level. As a result, we believe that up-converted SPDC, which has been shown to contribute broadband noise to frequency conversion [45,50], is not the dominant noise source in our SFG configuration. We attribute the contrast in SNR between down-conversion and up-conversion primarily to the difference in detector sensitivity at the pump wavelength: the Si visible detector is sensitive to the pump wavelength, whereas the InGaAs IR detector is not. The resulting inability to detect pump light leaking through the filters during down-conversion and the commensurate lower noise level suggest that pump leakage is the dominant source of noise in the up-conversion configuration. This noise could in principle be removed by increasing the optical depth of the filters at the pump wavelength.

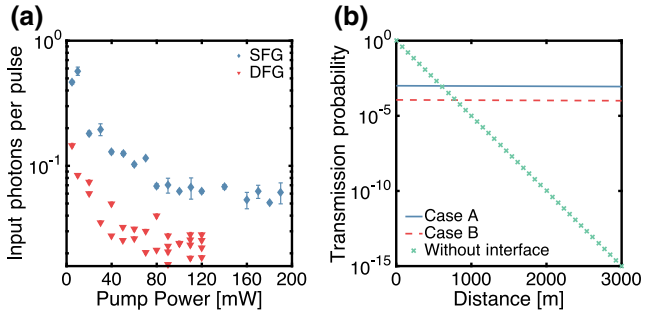

FIG. 4. (a) μ_1, the lowest possible number of photons per pulse to send into the device to get a SNR ≥ 1. (b) Probability of successful transmission of two photons from remote trapped Sr^+ ion processing nodes to an entangler along a fiber network with and without our interface.

Our values of $\mu_1 \ll 1$ demonstrate that low-noise operation is possible without narrow-band spectral filtering. Although high-efficiency conversion of nanosecond-duration photons from Sr^+ ions would require increased pulse energy, because of the broadband nature of the noise and its linear dependence on pulse energy, we expect that low-noise conversion could be maintained through narrow-band filtering as seen in [36,39]. To illustrate, we consider our device operation in ion compatible down-conversion, utilizing 1-μs-duration pump pulses. In our current configuration, we observe 3.9×10^{-6} noise photons per 300-ps pump pulse, at the point of highest conversion. Increasing pulse duration to 1 μs would see this number increase by a factor of approximately 3300. However, replacing our existing 8.9-nm band-pass filter at 1570 nm with a 200-MHz filter, similar to that used in [36], would see a reduction of broadband noise by a factor of approximately 5400, hence maintaining a similar noise contribution overall.

B. Projected network enhancement

In Fig. 4(b), we consider the end-to-end efficiency of three scenarios in which entanglement needs to be established between remote processing nodes, taking into account the transmission loss of the fiber at the wavelengths 422 and 1550 nm (< 50 dB/km for SM400 at 422 nm and < 0.18 dB/km for SMF-28 at 1550 nm). In case A, a violet photon from node 1 is down-converted via our interface and transmitted through a length of optical fiber before reaching the location of the second node, where it is up-converted to allow interference with a photon emitted directly from node 2. In case B, both photons emitted by the ion traps are down-converted before being transmitted through optical fiber and interfered with at some midway position. The final case is where no interface is used and a violet photon is emitted from one of the nodes before being

transmitted through fiber to the second node, whereupon an entanglement link is established. For each case, we present the probability of the photons successfully reaching their destination, assuming no coupling loss. We see that the use of our interface would drastically increase the probability of successful end-to-end transmission for remote nodes linked by fiber, even for typical intracity distances of a few kilometers.

V. CONCLUSION

We have implemented an interface capable of low-noise up- and down-conversion of single-photon-level light with efficiencies of 9.4% and 1.1%, respectively, in a custom-poled MgO:PPLN crystal. When considering the transmission loss of a single-mode fiber at the Sr^+ emission wavelength of 422 nm relative to that at 1550 nm, our interface would increase the probability of successful transmission of quantum information by 47 orders of magnitude over a distance of 10 km. We have demonstrated that the noise introduced when converting a weak coherent state is far below the level required to achieve high-fidelity operation with single photons emitted by trapped Sr^+ ions. Hence, we believe that our interface will enable long-distance entanglement distribution through chains of nodes containing trapped Sr^+ ions, paving the way for the construction of large-scale quantum networks. All data underlying the results presented in this manuscript can be found in Ref. [51].

ACKNOWLEDGMENTS

This work was funded by the UK EPSRC Quantum Technology Hub Networked Quantum Information Technologies, Grant No. EP/M013243/1. B.B. acknowledges funding from the European Union (EU) Horizon 2020 Research and Innovation Program under Grant No. 665148. P.M.L. acknowledges funding from the European Union Horizon 2020 Research and Innovation Framework Programme Marie Curie individual fellowship, Grant No. 705278.

[1] H. J. Kimble, The quantum internet, Nature **453**, 1023 (2008).

[2] L. M. Duan, M. D. Lukin, J. I. Cirac, and P. Zoller, Long-distance quantum communication with atomic ensembles and linear optics, Nature **414**, 413 (2001).

[3] Qi-Chao Sun, Yang-Fan Jiang, Ya-Li Mao, Li-Xing You, Wei Zhang, Wei-Jun Zhang, Xiao Jiang, Teng-Yun Chen, Hao Li, Yi-Dong Huang, Xian-Feng Chen, Zhen Wang, Jingyun Fan, Qiang Zhang, and Jian-Wei Pan, Entanglement swapping over 100 km optical fiber with independent entangled photon-pair sources, Optica **4**, 1214 (2017).

[4] Juan Yin, Yuan Cao, Yu-Huai Li, Ji-Gang Ren, Sheng-Kai Liao, Liang Zhang, Wen-Qi Cai, Wei-Yue Liu, Bo Li, Hui Dai, Ming Li, Yong-Mei Huang, Lei Deng, Li Li, Qiang Zhang, Nai-Le Liu, Yu-Ao Chen, Chao-Yang Lu, Rong Shu, Cheng-Zhi Peng, Jian-Yu Wang, and Jian-Wei Pan, Satellite-to-Ground Entanglement-based Quantum Key Distribution, Phys. Rev. Lett. **119**, 200501 (2017).

[5] C. J. Ballance, T. P. Harty, N. M. Linke, M. A. Sepiol, and D. M. Lucas, High-Fidelity Quantum Logic Gates using Trapped-Ion Hyperfine Qubits, Phys. Rev. Lett. **117**, 060504 (2016).

[6] Ian A. Walmsley and Joshua Nunn, Editorial: Building Quantum Networks, Phys. Rev. Appl. **6**, 040001 (2016).

[7] Ramil Nigmatullin, Christopher J. Ballance, Niel de Beaudrap, and Simon C. Benjamin, Minimally complex ion traps as modules for quantum communication and computing, New J. Phys. **18**, 103028 (2016).

[8] Prem Kumar, Quantum frequency conversion, Opt. Lett. **15**, 1476 (1990).

[9] Marius A. Albota and Franco N. C. Wong, Efficient single-photon counting at 1.55 m by means of frequency upconversion, Opt. Lett. **29**, 1449 (2004).

[10] Aiko Samblowski, Christina E. Vollmer, Christoph Baune, Jaromír Fiurášek, and Roman Schnabel, Weak-signal conversion from 1550 to 532 nm with 84% efficiency, Opt. Lett. **39**, 2979 (2014).

[11] Carsten Langrock, Eleni Diamanti, Rostislav V. Roussev, Yoshihisa Yamamoto, M. M. Fejer, and Hiroki Takesue, Highly efficient single-photon detection at communication wavelengths by use of upconversion in reverse-proton-exchanged periodically poled $LiNbO_3$ waveguides, Opt. Lett. **30**, 1725 (2005).

[12] S. Tanzilli, W. Tittel, M. Halder, O. Alibart, P. Baldi, N. Gisin, and H. Zbinden, A photonic quantum information interface, Nature **437**, 116 (2005).

[13] Hayden J. McGuinness, Michael G. Raymer, Colin J. McKinstrie, and Stojan Radic, Quantum Frequency Translation of Single-Photon States in a Photonic Crystal Fiber, Phys. Rev. Lett. **105**, 093604 (2010).

[14] Alex S. Clark, Shayan Shahnia, Matthew J. Collins, Chunle Xiong, and Benjamin J. Eggleton, High-efficiency frequency conversion in the single-photon regime, Opt. Lett. **38**, 947 (2013).

[15] Qing Li, Marcelo Davanco, and Kartik Srinivasan, Efficient and low-noise single-photon-level frequency conversion interfaces using silicon nanophotonics, Nat. Photonics **10**, 406 (2016).

[16] Xiang Guo, Chang-Ling Zou, Hojoong Jung, and Hong X. Tang, On-Chip Strong Coupling and Efficient Frequency Conversion between Telecom and Visible Optical Modes, Phys. Rev. Lett. **117**, 123902 (2016).

[17] A. G. Radnaev, Y. O. Dudin, R. Zhao, H. H. Jen, S. D. Jenkins, A. Kuzmich, and T. A. B. Kennedy, A quantum memory with telecom-wavelength conversion, Nat. Phys. **6**, 894 (2010).

[18] Philip J. Bustard, Duncan G. England, Khabat Heshami, Connor Kupchak, and Benjamin J. Sussman, Quantum frequency conversion with ultra-broadband tuning in a Raman memory, Phys. Rev. A **95**, 053816 (2017).

[19] Aaron P. Vandevender and Paul G. Kwiat, High efficiency single photon detection via frequency up-conversion, J. Mod. Opt. **51**, 1433 (2004).

[20] Christina E. Vollmer, Christoph Baune, Aiko Samblowski, Tobias Eberle, Vitus Händchen, Jaromír Fiurášek, and Roman Schnabel, Quantum Up-Conversion of Squeezed Vacuum States from 1550 to 532 nm, Phys. Rev. Lett. **112**, 073602 (2014).

[21] Dehuan Kong, Zongyang Li, Shaofeng Wang, Xuyang Wang, and Yongmin Li, Quantum frequency down-conversion of bright amplitude-squeezed states, Opt. Express **22**, 24192 (2014).

[22] Rikizo Ikuta, Yoshiaki Kusaka, Tsuyoshi Kitano, Hiroshi Kato, Takashi Yamamoto, Masato Koashi, and Nobuyuki Imoto, Wide-band quantum interface for visible-to-telecommunication wavelength conversion, Nat. Commun. **2**, 537 (2011).

[23] Nicolas Maring, Pau Farrera, Kutlu Kutluer, Margherita Mazzera, Georg Heinze, and Hugues de Riedmatten, Photonic quantum state transfer between a cold atomic gas and a crystal, Nature **551**, 485 (2017).

[24] Aaron P. Vandevender and Paul G. Kwiat, Quantum transduction via frequency upconversion (invited), JOSA B **24**, 295 (2007).

[25] T. Honjo, H. Takesue, H. Kamada, Y. Nishida, O. Tadanaga, M. Asobe, and K. Inoue, Long-distance distribution of time-bin entangled photon pairs over 100 km using frequency up-conversion detectors, Opt. Express **15**, 13957 (2007).

[26] Matthew T. Rakher, Lijun Ma, Oliver Slattery, Xiao Tang, and Kartik Srinivasan, Quantum transduction of telecommunications-band single photons from a quantum dot by frequency upconversion, Nat. Photonics **4**, 786 (2010).

[27] Matthew T. Rakher, Lijun Ma, Marcelo Davanco, Oliver Slattery, Xiao Tang, and Kartik Srinivasan, Simultaneous Wavelength Translation and Amplitude Modulation of Single Photons from a Quantum Dot, Phys. Rev. Lett. **107**, 083602 (2011).

[28] Nicolas Maring, Kutlu Kutluer, Joachim Cohen, Matteo Cristiani, Margherita Mazzera, Patrick M. Ledingham, and Hugues de Riedmatten, Storage of up-converted telecom photons in a doped crystal, New J. Phys. **16**, 113021 (2014).

[29] Christoph Baune, Jan Gniesmer, Sacha Kocsis, Christina E. Vollmer, Petrissa Zell, Jaromír Fiurášek, and Roman Schnabel, Unconditional entanglement interface for quantum networks, Phys. Rev. A **93**, 010302 (2016).

[30] Markus Allgaier, Vahid Ansari, Linda Sansoni, Christof Eigner, Viktor Quiring, Raimund Ricken, Georg Harder, Benjamin Brecht, and Christine Silberhorn, Highly efficient frequency conversion with bandwidth compression of quantum light, Nat. Commun. **8**, 14288 (2017).

[31] Hiroki Takesue, Single-photon frequency down-conversion experiment, Phys. Rev. A **82**, 013833 (2010).

[32] Sebastian Zaske, Andreas Lenhard, Christian A. Kessler, Jan Kettler, Christian Hepp, Carsten Arend, Roland Albrecht, Wolfgang-Michael Schulz, Michael Jetter, Peter Michler, and Christoph Becher, Visible-to-Telecom Quantum Frequency Conversion of Light from a Single Quantum Emitter, Phys. Rev. Lett. **109**, 147405 (2012).

[33] Kristiaan De Greve, Leo Yu, Peter L. McMahon, Jason S. Pelc, Chandra M. Natarajan, Na Young Kim, Eisuke Abe, Sebastian Maier, Christian Schneider, Martin Kamp, Sven Höfling, Robert H. Hadfield, Alfred Forchel, M. M. Fejer, and Yoshihisa Yamamoto, Quantum-dot spin-photon entanglement via frequency downconversion to telecom wavelength, Nature **491**, 421 (2012).

[34] Jason S. Pelc, Leo Yu, Kristiaan De Greve, Peter L. McMahon, Chandra M. Natarajan, Vahid Esfandyarpour, Sebastian Maier, Christian Schneider, Martin Kamp, Sven Höfling, Robert H. Hadfield, Alfred Forchel, Yoshihisa Yamamoto, and M. M. Fejer, Downconversion quantum interface for a single quantum dot spin and 1550-nm single-photon channel, Opt. Express **20**, 27510 (2012).

[35] Boris Albrecht, Pau Farrera, Xavier Fernandez-Gonzalvo, Matteo Cristiani, and Hugues de Riedmatten, A waveguide frequency converter connecting rubidium-based quantum memories to the telecom C-band, Nat. Commun. **5**, 3376 (2014).

[36] Pau Farrera, Nicolas Maring, Boris Albrecht, Georg Heinze, and Hugues de Riedmatten, Nonclassical correlations between a C-band telecom photon and a stored spin-wave, Optica **3**, 1019 (2016).

[37] V. Krutyanskiy, M. Meraner, J. Schupp, and B. P. Lanyon, Polarisation-preserving photon frequency conversion from a trapped-ion-compatible wavelength to the telecom C-band, Appl. Phys. B **123**, 228 (2017).

[38] Matthias Bock, Pascal Eich, Stephan Kucera, Matthias Kreis, Andreas Lenhard, Christoph Becher, and Jürgen Eschner, High-fidelity entanglement between a trapped ion and a telecom photon via quantum frequency conversion, arXiv:1710.04866v1 (2017).

[39] Thomas Walker, Koichiro Miyanishi, Rikizo Ikuta, Hiroki Takahashi, Samir Vartabi Kashanian, Yoshiaki Tsujimoto, Kazuhiro Hayasaka, Takashi Yamamoto, Nobuyuki Imoto, and Matthias Keller, Long-distance single photon transmission from a trapped ion via quantum frequency conversion, arXiv:1711.09644 (2017).

[40] Anaïs Dréau, Anna Tchebotareva, Aboubakr El Mahdaoui, Cristian Bonato, and Ronald Hanson, Quantum frequency conversion to telecom of single photons from a nitrogen-vacancy center in diamond, arXiv:1801.03304v1 (2018).

[41] Ryan Clark, Taehyun Kim, and Jungsang Kim, in *2011 IEEE Photonics Society Summer Topical Meeting Series, Montreal, QC, Canada* (IEEE, 2011), p. 45.

[42] S. Wang, V. Pasiskevicius, F. Laurell, and H. Karlsson, Ultraviolet generation by first-order frequency doubling in periodically poled $KTiOPO_4$, Opt. Lett. **23**, 1883 (1998).

[43] Daniel B. Oh, Diode-laser-based sum-frequency generation of tunable wavelength-modulated UV light for OH radical detection, Opt. Lett. **20**, 100 (1995).

[44] Helge Rütz, Kai-Hong Luo, Hubertus Suche, and Christine Silberhorn, Towards a quantum interface between telecommunication and UV wavelengths: Design and classical performance, Appl. Phys. B **122**, 13 (2016).

[45] Helge Rütz, Kai-Hong Luo, Hubertus Suche, and Christine Silberhorn, Quantum Frequency Conversion between Infrared and Ultraviolet, Phys. Rev. Appl. **7**, 024021 (2017).

[46] Y. O. Dudin, A. G. Radnaev, R. Zhao, J. Z. Blumoff, T. A. B. Kennedy, and A. Kuzmich, Entanglement of Light-Shift

Compensated Atomic Spin Waves with Telecom Light, Phys. Rev. Lett. **105**, 260502 (2010).

[47] Mustafa Gündoğan, Patrick M. Ledingham, Kutlu Kutluer, Margherita Mazzera, and Hugues de Riedmatten, Solid State Spin-Wave Quantum Memory for Time-Bin Qubits, Phys. Rev. Lett. **114**, 230501 (2015).

[48] O. A. Louchev, N. E. Yu, S. Kurimura, and K. Kitamura, Thermal inhibition of high-power second-harmonic generation in periodically poled $LiNbO_3$ and $LiTaO_3$ crystals, Appl. Phys. Lett. **87**, 131101 (2005).

[49] J. S. Pelc, L. Ma, C. R. Phillips, Q. Zhang, C. Langrock, O. Slattery, X. Tang, and M. M. Fejer, Long-wavelength-pumped upconversion single-photon detector at 1550 nm: Performance and noise analysis, Opt. Express **19**, 21445 (2011).

[50] Lichun Meng, Andreas Fix, Martin Wirth, Lasse Hgstedt, Peter Tidemand-Lichtenberg, Christian Pedersen, and Peter John Rodrigo, Upconversion detector for range-resolved DIAL measurement of atmospheric CH_4, Opt. Express **26**, 3850 (2018).

[51] https://doi.org/10.15125/BATH-00546.